

Received January 13, 2021, accepted February 5, 2021, date of publication February 9, 2021, date of current version February 18, 2021.

Digital Object Identifier 10.1109/ACCESS.2021.3058083

# Partial Discharges in Electrical Machines for the More Electric Aircraft—Part I: A Comprehensive Modeling Tool for the Characterization of Electric Drives Based on Fast Switching Semiconductors

MARCO PASTURA<sup>1</sup>, STEFANO NUZZO<sup>1</sup>, (Member, IEEE),  
FABIO IMMOVILLI<sup>1</sup>, (Senior Member, IEEE), ANDREA TOSCANI<sup>2</sup>,  
ALBERTO RUMI<sup>3</sup>, (Student Member, IEEE), ANDREA CAVALLINI<sup>3</sup>, (Senior Member, IEEE),  
GIOVANNI FRANCESCHINI<sup>1</sup>, AND DAVIDE BARATER<sup>1</sup>, (Member, IEEE)

<sup>1</sup>Department of Engineering “Enzo Ferrari”, University of Modena and Reggio Emilia, 41121 Modena, Italy

<sup>2</sup>Department of Engineering and Architecture, University of Parma, 43121 Parma, Italy

<sup>3</sup>Department of Electrical, Electronic and Information Engineering “Guglielmo Marconi”, University of Bologna, 40126 Bologna, Italy

Corresponding author: Stefano Nuzzo (stefano.nuzzo@unimore.it)

This work was supported by the Clean Sky 2 Joint Undertaking under the European Union’s Horizon 2020 research and innovation programme under Grant 785513, for the Reliable Aircraft electrical Insulation System sElection (RAISE) project.

**ABSTRACT** The arrival on the market of new power devices based on wide bandgap semiconductors has raised a relevant interest due to their superior properties compared to conventional technologies. On the other hand, these devices are inherently characterized by high rates of voltage changes over time, which may result in reliability challenges in electric drives adopting them. In fact, dangerous voltage overshoots at the motor terminals and uneven voltage distributions within the machine windings may occur. These phenomena can trigger a high insulation stress and partial discharges and, as a consequence, they may concur to the premature failure of the dielectric materials. This paper proposes a flexible and comprehensive modelling approach for the accurate analysis and estimation of both voltage overshoots and voltage distributions in a typical converter-cable-motor system intended for more electric aircraft applications. The modelling results are validated against experimental measurements carried out on a physical prototype comprising a wide bandgap-based converter, a connecting cable and an electrical machine stator. The findings are then used in the companion papers (part II and part III) to investigate the dependence of partial discharge phenomena on these voltage waveforms, highlight reliability challenges in modern  $\pm 270$  V DC bus voltage drives for the more electric aircraft and discuss solutions.

**INDEX TERMS** Electric drives, electrical machines, insulation, insulation stress, more electric aircraft, partial discharges, reliability, voltage distribution, voltage overshoot, wide bandgap.

## I. INTRODUCTION

Usually, power appliances are designed to operate with input voltage within 10% of the rated nominal value. All other voltage excitations may be seen as transients, which may arise from abnormal conditions, such as: short-circuits, switching operations, lightning discharges, and from almost any change in the operating conditions of the system. There are exceptions, for example, electrical machines fed through pulse width modulation (PWM) voltage source converters, since

The associate editor coordinating the review of this manuscript and approving it for publication was Jenny Mahoney.

these produce steep voltage pulses which are applied repeatedly to the machine terminals [1]. The inverters may produce voltages with very short rise times, which in presence of long cables may increase the electrical stress significantly, leading to partial discharge inception and to the stator insulation failure in a short time.

In general, standards classify the transient voltages that power equipment experiences into four groups [2], including:

1. Low-frequency transients, which are oscillatory voltages (from power frequency to a few kHz), weakly damped and of relatively long duration (i.e., seconds, or even minutes).

2. Slow front transients, which refer to excitations caused by switching operations, fault initiation, or remote lightning strokes. They can be oscillatory (within a frequency range between power frequency and 20 kHz) or unidirectional (with a front time between 0.02 and 5 ms), highly damped and of short-duration (i.e., in the order of milliseconds).
3. Fast front transients, which are normally aperiodic waves, generally associated to lightning surges with a front time between 0.1 and 20  $\mu$ s.
4. Very fast front transients, referring to surges with rise times in the range up to 100 ns and frequencies from 0.5 to 30 MHz.

The capability of a winding to withstand transient voltages depends on the specific surge voltage shape, the winding geometry, the insulation material, the voltage-time withstand characteristic and the past history of the winding [3], [4].

Transients cause both overvoltages at the machine terminals [5] and uneven voltage distributions within machine windings [6]. These result in increased local thermal and electric stress on the insulation system and additional losses, which in turn cause an accelerated degradation of the insulation and of its electrical properties [7]. Stator insulation failure is one of the main reasons for machine breakdowns and the introduction of power converters utilizing wide bandgap (WBG) devices, based on Silicon Carbide (SiC) or Gallium Nitride (GaN), further increase the electrical stress due to their faster rise times compared to traditional Si-based switching devices.

#### A. METHODS FOR THE PREDICTION OF VOLTAGE OVERSHOOT AT MACHINE TERMINALS

Voltage overshoots at machine terminals are linked to the high frequency (HF) behavior of the system, so HF models of the components of the whole system, in particular of the feeding cable and the machine, are mandatory. There are two typical approaches used for the development of such models: the finite element (FE) analysis [8] and the direct measurement through an RLC meter [9] or an impedance analyzer [10]. FE models can be rather time consuming: in fact, while a 2D approximation of the field problem is usually sufficient for the cable [11], a full 3D analysis may be required for the electrical machine. Hence, when the electrical motor is available, the equivalent parameters extraction is carried out through impedance measurement.

While the electrical machine's models always consist in lumped-parameters ones [8]–[12], the cable can be represented either through transmission lines [10] or with a series of sufficiently short lumped sections [9], approximating a distributed parameter line. For both cases, the per unit length impedances (stray capacitances, inductances and resistances) need to be extracted. It is clear that the accuracy for the voltage overshoot estimation depends on both the modeling approach and the parameter extraction. The machine phase-to-phase overvoltage corresponds to the differential

mode (DM) behavior of the system. Hence, rather than using three-phase models [11], its estimation can be carried out via equivalent single-phase DM models [10], thus saving simulation times without significantly compromising the accuracy.

#### B. METHODS FOR THE PREDICTION OF THE VOLTAGE DISTRIBUTION WITHIN MACHINE WINDINGS

The uneven voltage distribution process occurring in electrical machines has been investigated for both form-wound [13], [14] and random-wound windings [15], [16]. While in form-wound coils the interturn voltages are not so critical due to the sequential winding location, random-wound windings can have significant effects on the parasitic parameters' values [16]. A classical way to model such phenomenon is based upon multi-conductor transmission line theory [17], where the relative electrical parameters can be calculated either using simplified analytical approaches [16] or more accurate FE evaluations [15]–[19]. Depending on the objectives of a specific research activity, the equivalent circuits usually implemented for estimating the voltage stress within windings can be complex and the estimation of the circuitual parameters can be computationally expensive. Therefore, usually some mutual parameters (e.g. mutual capacitances between turns) are neglected, dielectric losses are not taken into account and the calculations are made for one frequency only [15], [19], [20]. In specific applications, e.g. when front transients are not very fast, losses cannot be neglected [21] and sometimes a frequency-domain modelling approach may be needed [22].

#### C. OBJECTIVE AND CONTRIBUTION

The previous subsections prove that a number of “uncoupled” modelling approaches are adopted for the estimation of overvoltages at the machine terminals (Section I.A) and of the voltage distribution within windings (Section I.B). This means that previous investigations have always examined these two main voltage stress sources separately, so that the output of such models is either the overvoltages at machine terminals or the voltage distribution across windings. This paper proposes a coupled and fully comprehensive methodology which is able to provide information regarding both these quantities, simultaneously. This is done using the output quantity of the overvoltage estimation model as the input for the voltage distribution model, whereas the available literature has never considered the effects of the voltage overshoots on the interturn voltages.

The tool can represent a powerful means to ensure a reliable design of electric drives employing converters with fast switching devices such as SiC and GaN. This is especially important in the aerospace field, where there is an ever-increasing need for HF operations, on one side, and for elevated reliability levels, on the other hand [23], [24]. The proposed modelling approach can be used to estimate the impact of the electrical aging on the electrical machine insulation system when its output quantities (i.e. overvoltages and voltage distributions) are considered as electrical input

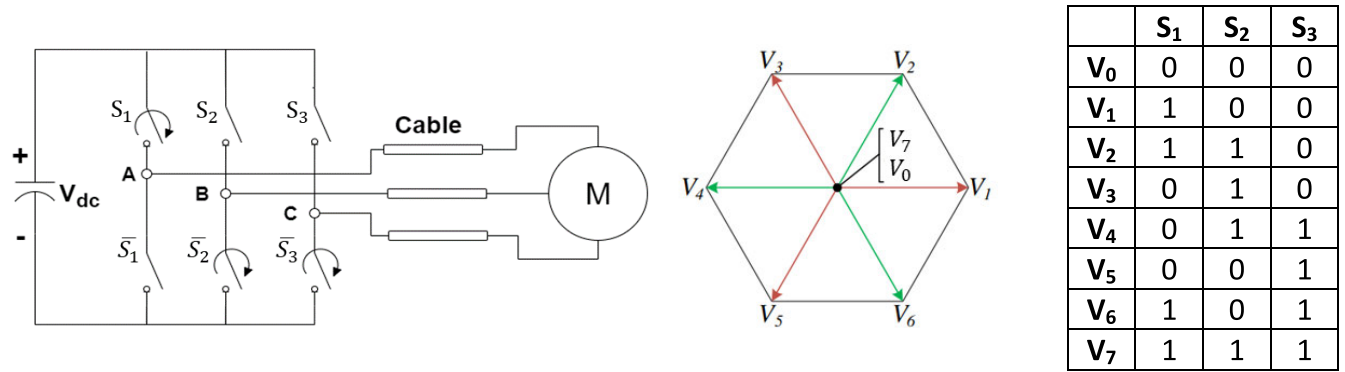


**FIGURE 1.** Inverter, cable and machine scheme: commutation of the inverter from state [0 0 0] to [1 0 0]. The current path sees the parallel of phase B and C in series to phase A.

parameters in an opportunely built lifetime model. Thanks to its flexibility and computation speed, the combined model will be used in part II to quantify the effects of WBG devices on partial discharge inception voltage (PDIV) through a number of parametric simulations, where the impact of different rise times and cable lengths are investigated. Finally, in part III the results from this part I will be employed to propose recommendations for PD prevention.

## II. CONVERTER-CABLE-MACHINE MODEL

The voltage waveforms provided by WBG devices can reach very high voltage gradients ( $dV/dt$ ), even higher than 20 kV/ $\mu$ s. The associated HF harmonics have a significant impact on the maximum voltage value at machine terminals. The wavelength of an electromagnetic wave is inversely proportional to its frequency, so at frequencies in the order of a few MHz the wavelength of these harmonics is comparable or smaller than the cable length, even for a few meters' cable. If a voltage pulse is applied to a cable of sufficient length, forward and backward travelling waves occur. These travel at a speed  $v = 1/\sqrt{L_0C_0}$ , where  $L_0$  and  $C_0$  are the per-meter inductance and capacitance of the cable. Another important parameter is the cable characteristic impedance, which is defined as the ratio between the forward travelling voltage wave and the corresponding current wave. At very HF, the characteristic impedance can be simplified as  $Z_0 = \sqrt{L_0/C_0}$  [25]. The behavior of the system strongly depends on  $v$  and  $Z_0$ . However, also the cable length and the characteristic impedance  $Z_m$  of the electrical machine supplied by the PWM pulses play a significant role. The so-called reflected wave occurs when there is an impedance mismatch between feeding cable and electrical machine. Since  $Z_0$  and  $Z_m$  are usually rather different a reflection appears, giving rise to a certain overvoltage. The reflection coefficient is defined as in (1) and the maximum theoretical voltage  $V_m$  (i.e. when a full reflection occurs) at machine terminals is as in (2), where  $V_{in}$  is the voltage applied at the beginning of the line [25], [26].

$$\Gamma = \frac{Z_m - Z_0}{Z_m + Z_0} \quad (1)$$

$$V_m = V_{in} (1 + \Gamma) \quad (2)$$

Typically,  $Z_m \gg Z_0$  [25], [26], so  $V_m$  can reach up to twice  $V_{in}$ . A full reflection happens when the cable is longer than the critical length  $l_{cr}$  of the system, which is a function of  $v$  and the pulse rise time  $t_r$ , i.e.  $l_{cr} = v \cdot t_r/2$ . The equivalent mathematical condition for which there is a full reflection is  $t_r < 2 \cdot t_p$ , where  $t_p$  is the propagation time of the applied pulse. Nevertheless, a full reflection can occur also for  $t_r < 3 \cdot t_p$  [26] and the voltage at the machine terminals, under particular conditions, can be even higher than twice  $V_{in}$  [25].

As mentioned in Section I.A, the overvoltage can be analyzed through a DM model. The proposed model replicates the system behavior when the inverter, driven by space vector modulation, has an output transition from state  $V_0$  (0,0,0) to state  $V_1$  (1,0,0) (see Fig. 1).

This assumption is valid considering that for a 2-levels inverter only 3 switches are working at the same time, providing in state S1 a current path with one phase (e.g. A) connected in series to the parallel of the other two phases (e.g. B and C). A voltage source, generating the converter output voltage, and HF cable and machine models connected together realize the equivalent DM circuit for line-to-line voltage evaluations.

### A. CONVERTER

The converter is modelled as black-box, providing the output voltage. For preliminary investigations, the converter is modelled as an ideal DM voltage source providing an output voltage whose amplitude, rise time, frequency and duty cycle can be customized for every simulation, allowing to perform sensitivity analyses on the system behavior at different supply conditions.

### B. CABLE

The HF model of the feeding cable is based on [10], which determines the equivalent cable parameters through impedance measurement for different frequency values. However, some updates and modifications are applied in this work. The equivalent longitudinal parameters are not lumped

only in the supply path (phase A), but also in the return path (phase B in parallel to phase C), as seen in Fig. 2. The parameters for the phase A have been estimated and then DM connection has been applied. The phase A equivalent longitudinal parameters (i.e.  $R_{s1}$ ,  $L_{s1}$ ,  $R_{s2}$  and  $L_{s2}$ ) are referred to the supply path (i.e. single-phase connection), while the same parameters are divided by two for the return path, since phases B and C are in parallel.  $R_{s1}$  and  $L_{s1}$  are respectively the equivalent resistance and inductance which model the low-medium frequency behavior of the cable short circuit impedance, while  $R_{s2}$  and  $L_{s2}$  are representative of the HF behavior, where the influence of skin and proximity effects are higher. The transversal parameters (i.e.  $Z_{p1}$  and  $Z_{p2}$ ) dominate the open circuit impedance behavior and take into account the dielectric losses, the inter-phase capacitance and conductance. The measurements are carried out at 1) open circuit for the estimation of the transversal parameters  $Z_{p1}$  and  $Z_{p2}$ , and 2) short-circuit for the extraction of the longitudinal parameters. The determined parameters have been verified using MatLab Simulink, where a model like the one reported in Fig. 2 has been built. In the short circuit simulation, terminals 3 and 4 have been connected together, while they are left floating in the open circuit simulation. Figures 3 and 4 show the comparison between the measured DM longitudinal and transversal impedances of a single cable section and the corresponding impedances provided by the model with the estimated impedance parameters. An excellent match is observed for the whole range of the considered frequencies between the measured data and the fitted ones. Further details of the cable topology will be provided in Section IV.

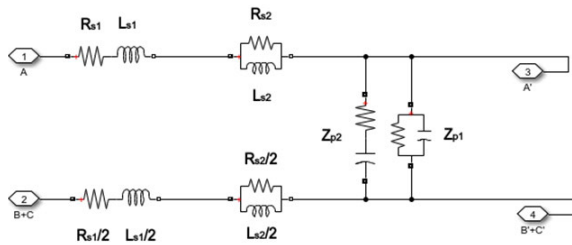


FIGURE 2. 1 m section of the DM cable model.

C. ELECTRICAL MACHINE

After an intense literature survey, the machine equivalent circuit model is taken as that of Fig. 5 [10] due to its ease of implementation.

The equivalent parameters have been calculated similarly to the methods adopted for the cable, starting from impedance measurement in the low-to-high frequency range and following the procedure detailed in [10]. The machine parameters are  $L_d$ ,  $R_e$ ,  $R_t$ ,  $L_t$ ,  $C_t$ ,  $R_{g1}$ ,  $C_{g1}$ ,  $R_{g2}$  and  $C_{g2}$ .  $L_d$  represents the stator winding leakage inductance;  $R_e$  is the equivalent resistance which takes into account the ferromagnetic losses;  $R_t$ ,  $L_t$ ,  $C_t$  are necessary to capture the HF resonances;  $R_{g1}$ ,  $R_{g2}$ ,  $C_{g1}$  and  $C_{g2}$  are the parasitic impedances towards the stator frame and influence the CM behavior of the machine.

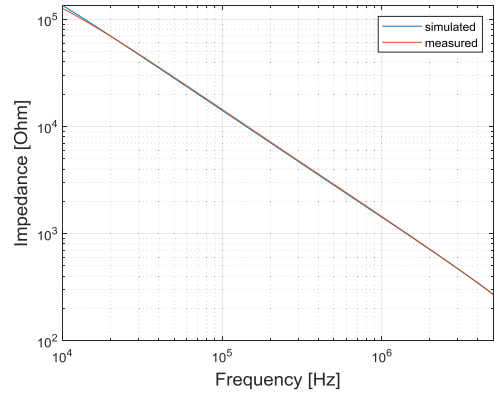


FIGURE 3. DM short circuit impedance of 1m cable section-comparison between simulated and measured results.

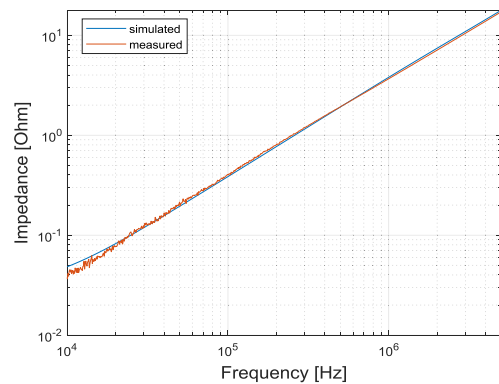


FIGURE 4. DM open circuit impedance of 1m cable section-comparison between simulated and measured results.

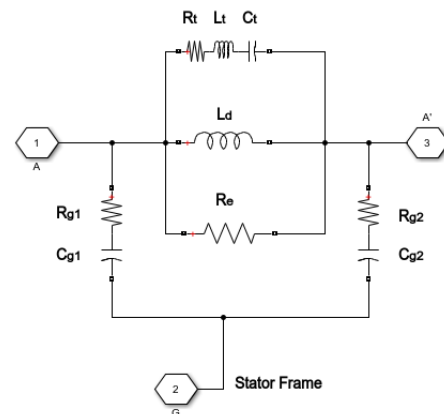
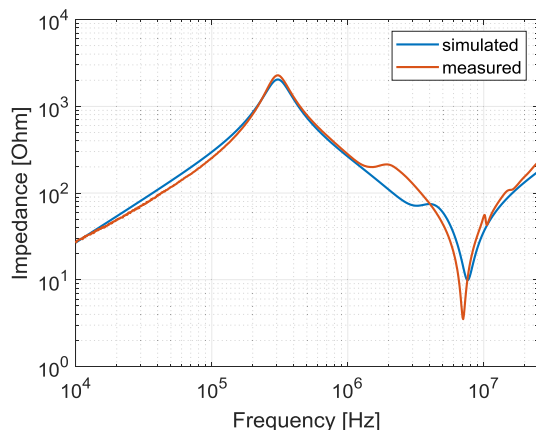


FIGURE 5. Single-phase, HF model of the electrical machine.

After estimation of these equivalent parameters, a DM connection is applied for both verification of the impedance as a function of frequency and for time domain overvoltage simulations. The frequency DM response can be observed in Fig. 6, where again a very good match between simulated and measured results can be appreciated. However, some discrepancies can be observed above 1 MHz, probably due to possible inaccuracies at very HF, where the equivalent



**FIGURE 6.** DM impedance of the electrical machine – comparison between simulated and measured results.

parasitic impedances can become comparable to the parasitic impedances of measurement apparatus.

### III. VOLTAGE DISTRIBUTION MODEL

While for system-level studies it is sufficient to model the component as a black-box model, when the internal transient response is required, a much more detailed model in which all regions of critical dielectric stress are identified needs to be used. Internal transient response is a result of the distributed electrostatic and electromagnetic characteristics of the windings. For a steep-fronted voltage surge, most of the wave front will reside across the first few turns, which can be overstressed. The wave front slopes off and the amplitude is attenuated as the wave penetrates along the winding. For all practical winding structures, this phenomenon is relatively complex and can only be investigated by constructing a detailed model and carrying out a numerical solution for the transient response and frequency characteristics in the regions of concern. An accurate model may consider each turn of the winding represented by capacitances, inductances and resistances [3], [4]. Winding capacitances play a vital role in establishing the initial voltage distribution along the winding when a steep-fronted voltage is suddenly applied.

#### A. ASSUMPTIONS

The machine winding consists of a chain of series-connected coils that are distributed around the machine stator. Under steep-fronted transient conditions, the effective self-inductance of a coil differs considerably from the 50 Hz value. Initially, the self-inductance arises from flux that is confined mainly to paths outside the high-permeability iron core by eddy currents that are set up in the core by the incident surge. The reluctance of the flux paths changes as the flux penetrates into the core. Similar considerations apply to the mutual coupling between coils. However, due to the limited extent of flux penetration into the core, the flux linkage from one coil to a coil in a neighboring slot is very small, so the mutual coupling between coils under surge voltage conditions

is also very small. The capacitance between coils is very low because each coil is embedded in a slot which acts as a grounded boundary. The intercoil capacitance is usually limited to that in the line-end coil and is very small too. However, due to the fact that the coil is embedded in the slot, the coil-to-ground is significant [17].

Considering all the above, the following assumptions can be made when deriving the equivalent circuit of a machine winding:

- The behavior of the core iron is like that of a grounded sheath and the slot iron boundary may be replaced by a grounded sheath, which is impenetrable to HF waves.
- The series inductance and resistance of the coils are frequency dependent due to the eddy currents in the core and to the skin effect in conductors.
- Only transverse electromagnetic (TEM) propagation mode is considered, so the theory of multi-conductor transmission lines can thus be applied [17].
- The basic unit in the equivalent circuit for the winding is a coil.
- The two opposite overhang parts of the stator core are considered uncoupled because eddy-currents in the core provide effective shielding at high frequencies.
- Overhang and slot parts are also uncoupled because of the eddy current in the core.
- The two parts of the coil at the coil entry are uncoupled since they are nearly perpendicular to each other over most of their length and are further shielded from each other by eddy currents in adjacent coils.
- Insulation between the lamination permits magnetic coupling to the coils inside adjacent slots. However, the two slot parts of the coil are not coupled because of the eddy current in the neighbouring coils.
- Coupling between adjacent coils of different slot layers has a lower effect than the coupling between adjacent turns.
- The capacitive couplings between coils of one phase winding, and between coils of different phase windings, are very small and are thus neglected.
- The capacitance between turns in a coil and between the coil and the core are important and should be taken into account.

In conclusion, each turn of the coil may be modelled as a single conductor transmission line coupled to its neighbor turns.

#### B. CIRCUITAL APPROACH

##### 1) LUMPED-PARAMETER MODEL

The active sides of a single turn can be represented by series resistances (i.e.  $R_{i,i}$ ) and inductances (i.e.  $L_{i,i}$ ) with mutual inductances between turns (i.e.  $L_{i,j}$ ), and parallel (i.e.  $C_{ig}$ ) and series (i.e.  $C_{i,j}$ ) capacitances arranged as in Fig. 7. Resistances in parallel to these capacitances should be also included in such a network to model the dielectric losses accurately. However, when conventional impulse waves are

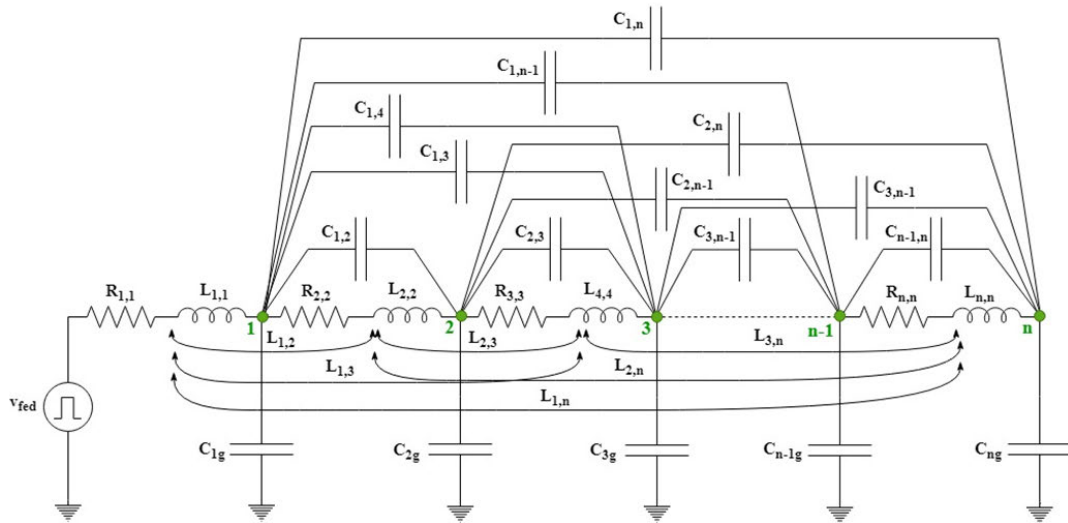


FIGURE 7. Equivalent lumped-parameter circuit of a machine coil.

applied, the peak voltage normally occurs on the first major oscillation and the error incurred by not modelling the winding loss is rather small. For these reasons, this study is carried out without including the loss model.

Considering all the assumptions mentioned in Section III.A, all of the 3D effects are neglected in first approximation and therefore the whole model coincides with that shown in Fig. 7. Additional reduction of the network may not yield useful results for transient voltage investigations.

## 2) GOVERNING EQUATIONS AND MODEL IMPLEMENTATION

It is clear that any electrical circuit software can be used to solve the network of Fig. 7, however this would be manageable only when the number of nodes is limited and, most importantly, it would not be flexible since a different network should be built every time the number of nodes (i.e. the number of conductors in the slot) needs to be modified. Hence, the lumped-parameter model should be solved using any numerical tool irrespectively of its number of elements and nodes. This is done by first developing the state-variable formulation which can be used to approximate the behavior of a machine winding in HF transients, and then by implementing the obtained expressions in MatLab Simulink environment.

Referring to the circuit of Fig. 7, only the input voltage  $v_{fed}$  is known and it corresponds to the surge voltage feeding the winding. At any node  $i$  of the network made of  $n$  nodes, the Kirchhoff's current law can be applied thus obtaining (3). In (3),  $i_i$  and  $i_{i+1}$  indicate the currents entering the nodes  $i$  and  $i + 1$  respectively,  $v_i$  is the voltage across  $C_{gi}$  and  $v_k$  that across all of the  $C_{ik}$  comprised in the circuit, with  $k \neq i$  and ranging from 1 to  $n$ .

$$i_i - i_{i+1} - C_{ig} \frac{dv_i}{dt} - \sum_{\substack{k=1 \\ k \neq i}}^n C_{i,k} \frac{d(v_i - v_k)}{dt} = 0 \quad (3)$$

Always referring to the circuit of Fig. 7, the Kirchhoff's voltage law can be applied to any loop including two adjacent node-to-ground capacitances, i.e.  $C_{i,g}$  and  $C_{i+1,g}$ , and the series parameters  $R_{i,i}$  and  $L_{i,i}$ . The expression (4) is thus obtained and provided below. The Kirchhoff's voltage law needs to be used also for the additional loop including  $v_{fed}$ ,  $R_{i,i}$ ,  $L_{i,i}$  and  $C_{I,g}$ , thus resulting still in (4), if one assumes that when  $i = 1$ , then  $v_{i-1} = v_{fed}$ .

$$v_{i-1} - v_i - R_{i,i}i_i - L_{i,i} \frac{di_i}{dt} - \sum_{\substack{k=1 \\ k \neq i}}^n L_{i,k} \frac{di_k}{dt} = 0 \quad (4)$$

From (3) and (4), it can be noticed that the system state variables are the currents entering in each node and the voltages across the node-to-ground capacitances of the network. To tidily group the state variables in two independent vectors, namely  $\bar{i} = (i_1 \ i_2 \ \dots \ i_n)^T$  and  $\bar{v} = (v_1 \ v_2 \ \dots \ v_n)^T$ , (3) and (4) can be firstly elaborated as in (5) and (6), respectively.

$$i_i - i_{i+1} = \left( C_{ig} + \sum_{\substack{k=1 \\ k \neq i}}^n C_{i,k} \right) \frac{dv_i}{dt} - \sum_{\substack{k=1 \\ k \neq i}}^n C_{i,k} \frac{dv_k}{dt} \quad (5)$$

$$v_{i-1} - v_i = R_{i,i}i_i + L_{i,i} \frac{di_i}{dt} + \sum_{\substack{k=1 \\ k \neq i}}^n L_{i,k} \frac{di_k}{dt} \quad (6)$$

After a few manipulations, the final expressions can be written in the state form given in (7) and III-C. Here,  $C_{sw}$  is a matrix of capacitances having the terms  $C_{ig} + \sum_{\substack{k=1 \\ k \neq i}}^n C_{i,k}$  on its main diagonal and all the terms  $-C_{i,k}$  in the corresponding positions  $i,k$  of the matrix,  $R$  is a diagonal matrix whose elements are the series resistances  $R_{i,i}$ ,  $L$  is the matrix having self-inductances  $L_{i,i}$  on the main diagonal and mutual-inductances  $L_{i,k}$  in the corresponding positions  $i,k$ .

In (7) and III-C, to achieve the state form and to allow for a compact description of the equations, the vector  $\bar{v}_{fed} = (v_{fed} \ 0 \ \dots \ 0)^T$  and the matrix  $\mathbf{D}$  are newly introduced. The latter matrix has all the elements of the main diagonal equal to -1, all the elements in the first sub-diagonal equal to 1 and all of the remaining elements equal to 0.

$$\frac{d\bar{v}}{dt} = \mathbf{C}_{sw}^{-1} \left( -\mathbf{D}^T \bar{i} \right) \quad (7)$$

$$\frac{d\bar{i}}{dt} = \mathbf{L}^{-1} \left( \bar{v}_{fed} + \mathbf{D} \bar{v} - \mathbf{R} \bar{i} \right) \quad (8)$$

The above equations are implemented in Matlab-Simulink environment, while the values of all of the elements included in the matrices  $\mathbf{R}$ ,  $\mathbf{L}$  and  $\mathbf{C}_{sw}$ , are determined through 2D finite element (FE) modeling of one machine slot. Their detailed description is provided in the next section.

### C. FINITE-ELEMENT MODELS

Given the complexity associated to an eventual analytical determination of resistances, inductances and capacitances, a FE analysis is chosen as means to do so. Considering all the assumptions and hypotheses described above in sections III.A and III.B, only one slot pitch is modelled. The electric field simulation software ElecNet is used to find the capacitances, whereas the low-frequency electromagnetics simulation software MagNet is employed for resistances and inductances. Apart from some differences inherently related to the nature of the problems, most of the pre-processing and solving features (such as creation of the geometry, assignment of materials, meshing and simulation parameters, types of solvers, etc.) are common to both software. The one slot pitch models comprise all the relevant elements necessary for the analysis, including the slot itself, two half teeth, conductors, enamel, interturn insulation and slot liners.

A 2D solution mesh in ElecNet and the relevant electric field distribution are shown in Fig. 8 a) and Fig. 8 b) respectively, where some of the modelling details can be observed. Similarly, Fig. 9 a) and Fig. 9 b) report the solution mesh in MagNet and the relevant magnetic field distribution. The time-harmonic solver is chosen as the most suitable for the sake of this study. Time-harmonic simulations are performed at one specified frequency, and sources and fields are represented by complex phasors.

It is worth mentioning that, after completing these sets of FE evaluations, the determined circuital parameters (capacitances in ElecNet and resistances and inductances in MagNet) have to be first stored and then manipulated in Matlab in such a way to obtain the matrix  $\mathbf{C}_{sw}$ ,  $\mathbf{R}$  and  $\mathbf{L}$  necessary for the numerical resolution of the assumed equivalent circuit.

### D. SUMMARIZING REMARKS

The whole automated process is coded in Matlab and the relevant steps, ranging from the definition of the geometrical dimensions to the solution of the dynamic system, are provided below:

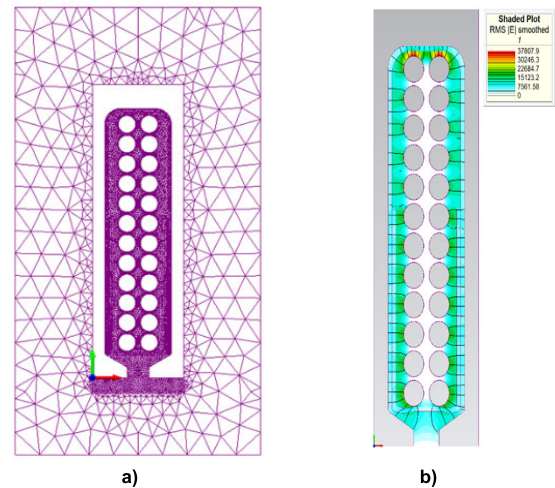


FIGURE 8. a) solution mesh and b) electric field distribution of the 2D FE slot pitch model developed in ElecNet.

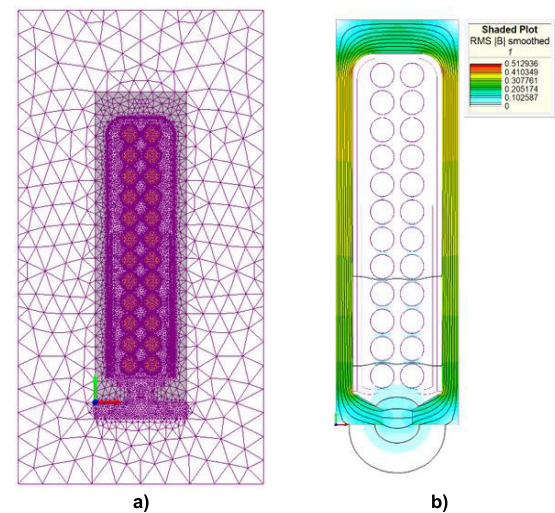


FIGURE 9. a) solution mesh and b) electric field distribution of the 2D FE slot pitch model developed in ElecNet.

1. The characteristic design parameters, such as slot dimensions, number of conductors, slot and conductor insulation thicknesses, etc. are defined in Matlab.
2. Matlab launches ElecNet, where the slot pitch model is built and simulations are performed to determine the capacitances.
3. Matlab launches MagNet, where the slot pitch model is built and simulations are performed to determine resistances and inductances.
4. The calculated equivalent circuit parameters are elaborated in Matlab in such a way to obtain the matrices  $\mathbf{R}$ ,  $\mathbf{L}$  and  $\mathbf{C}_{sw}$  needed for the system resolution.
5. The input parameters are defined for the voltage source  $v_{fed}$ .
6. Matlab launches Simulink, where the dynamic system model is built and the simulation is run, thus finding

the state variables, i.e. 1) turn currents and 2) node voltages.

- 1) Matlab post processes the results by plotting the obtained state variables.

The next section will describe the application of the models developed in Sections II and III to a specific electric drive case study. Finally, the two models will be coupled for the comprehensive analysis of the whole system.

#### IV. THE COMBINED MODEL

As mentioned above, the development of a comprehensive model able to estimate both overvoltages at the machine terminals and voltage distributions within windings represents the main contribution of this paper. So far, the two models have been described, developed and implemented separately. As such, they can be solved separately providing standalone information relative to overvoltages and interturn voltages. However, when the voltage distribution model was solved standalone, an ideal converter waveform would need to be hypothesized and the effects of the overvoltage on the voltage distribution would be inherently neglected [27]. As these phenomena are exacerbated in WBG-based drives, combining the two models is of paramount importance and represents an important progress beyond the state-of-the-art.

The inherent flexibility of such models allows for a straightforward merging and an easy and automatic communication within MatLab environment. The converter-cable-machine model estimates the voltage waveform at machine terminals, thus including overshoot and rise time. The latter is used to calculate the frequency at which the equivalent circuit parameters should be computed via FE analysis [19], while the terminal voltage waveform is used (i.e.  $v_{fed}$ ) for the voltage distribution Simulink model, thus allowing to compute node currents and voltages. The node voltages represent the turn-to-ground voltages which can be then post-processed to determine the interturn voltages. Figure 10 shows a simplified flow chart illustrating how the combined model (indicated as CCM, i.e. converter-cable-machine, and VD, i.e. voltage distribution) operate.

#### A. INVESTIGATION ON THE CASE STUDY

##### 1) DESCRIPTION OF THE CONSIDERED ELECTRIC DRIVE

The benchmark case study is a high-performance electric drive intended for a realistic more electric aircraft application. The basic structure of the system consists of an AC-DC converter directly connected to the on-board voltage supply, i.e. 230V AC at 360-800Hz, a DC-AC converter, with a DC-link voltage of 564V, which supplies via appropriate cabling a speed controlled electrical machine. The inverter is connected to the motor via a 6m three core cable using wire based on SAE AS 22759/41, with a diameter of 8AWG, twisted triple, single shielded (Nickel-coated copper), single jacket. Finally, the electrical machine has a rated continuous power of 5.7kW and is intended for continuous hydraulic power supply applications. It features an 8-poles, interior

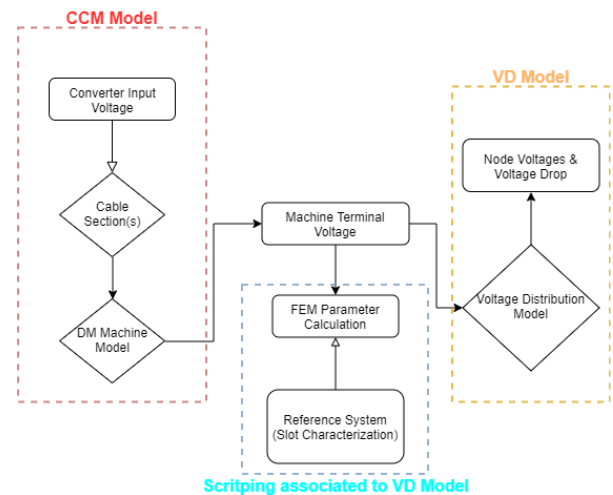


FIGURE 10. Simplified flow chart of the whole system model (i.e. merging of the two models).

TABLE 1. Electric drive main characteristics.

Machine	Application	Continuous hydraulic pump supply for MEA
	Topology	IPM
	Rated Power	5.7 kW
	Rated Voltage	230 V
	Frequency Range	360 - 800 Hz
	Slots	36
	Poles	8
	Winding type	Three-phase, double-layer
Converter	DC Bus Voltage	564 V
	SiC MOSFETs rating	900V, 11A
Cable	Length	6 m
	Topology	8 AWG Tripolar Shielded

permanent magnet (IPM) rotor and a 36-slots stator, with a double-layer, integer-slot, three-phase winding comprising 3 coils-per-pole-per-phase, each consisting of 12 turns. Table 1 summarizes the main characteristics of the electric drive under analysis.

##### 2) ADAPTION OF THE MODELS

The real shape of the benchmark stator slot is characterized by a trapezoidal layout, as typical in low power machines. On the other hand, the slot geometry assumed by the FE models is implemented by considering parallel sides for the sake of simplicity. In other words, a constant slot width has been considered and this is taken equal to the mid-segment of the trapezoid. Hence, the slot liners follow the parallel profiles of the slot sides. Apart from these adjustments, all the rest of the dimensions are identical to the benchmark machine.

Regarding the conductors, the effective number of turns, i.e. 12 turns per coil, is considered. The rest of the phase turns is modelled through a lumped ohmic-inductive impedance as



the interturn voltages are particularly significant on the first turns only.

### 3) PRELIMINARY RESULTS AND CONSIDERATIONS

Some preliminary simulations can be performed to assess the system behavior. For the given case study, a first investigation assumes that the converter output is as in Fig. 11 (blue waveform), i.e. a voltage ramp with an amplitude of 564 V and gradient equal to 20 kV/ $\mu$ s (rise time about 23 ns). Fig. 11 also shows the estimated voltage at the machine terminals, in red, featuring an overshoot nearly twice the converter output voltage amplitude (i.e. the DC link bus voltage) and a rise time  $t_r = 28$  ns. This results in a supply frequency of  $0.35/t_r = 12.5$  MHz being used for FE determination of resistances, inductances and capacitances.

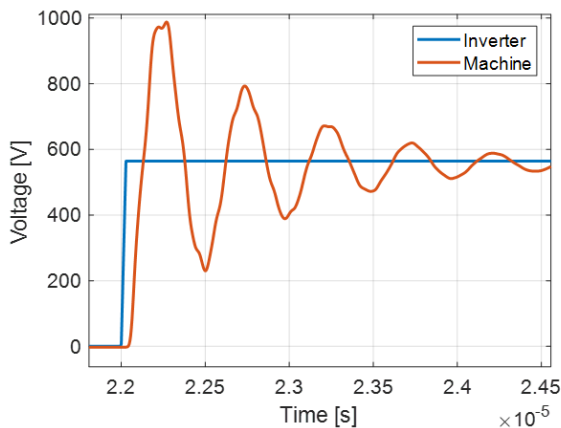


**FIGURE 11.** Machine line-to-line voltage (in red) ensuing from an inverter output voltage (in blue) of 564 V amplitude and 23 ns rise time.

Since the voltage at motor terminals is the result of the sum of an incident and reflected wave (which can be considered at first approximation as two first order responses), the supply frequency is computed basing on the bandwidth of a first order response. The resulting voltage distribution is obtained and reported in Fig. 12 for the first three turns, which are the most significant, proving that the voltage within windings is rather unevenly distributed.

## V. EXPERIMENTAL RESULTS

The aim of this last section is to prove that the validity and the accuracy of the proposed model by comparing the relevant results against experimental measurements carried out on a purposely-built prototype. First, the description of the experimental setup is provided and then the validation exercise is detailed.

### A. EXPERIMENTAL TEST SETUP

The experimental setup is built trying to replicate a typical electric drive for aerospace such as that described in Section IV.A. However, some modifications are applied to the benchmark system. A DC power supply unit (PSU) is used to

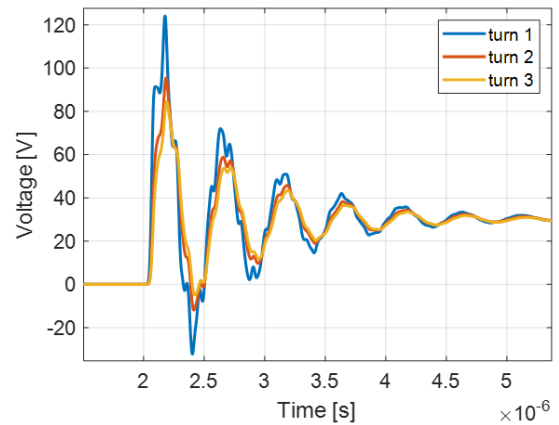


**FIGURE 12.** Voltage drop across the first three winding turns.

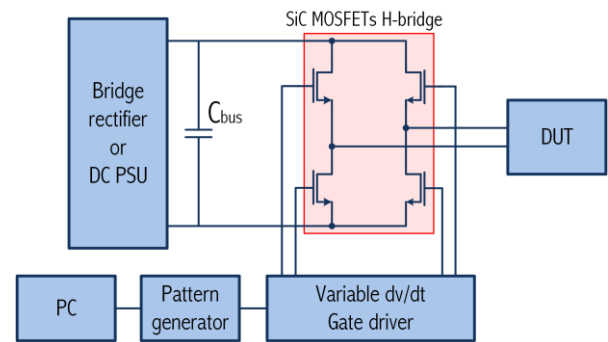


**FIGURE 13.** Block scheme of the experimental setup.

feed an H-bridge converter (Fig. 13), which is based on 900V, 11A SiC MOSFETs. The converter is linked to the electrical machine via a 6 m long cable, connected in DM. The SiC-based converter is equipped with variable  $dV/dt$  gate drivers allowing to investigate different supply conditions.

The motor features some accessible interturn terminals for voltage probing and only the stator is considered, thus inherently neglecting the rotor effects [19]. A Hall-effect current probe is used to measure the current and differential voltage probes are used to record the voltages (both at the machine terminals for the overshoot validation and at interturn terminals for the voltage distribution validation). All the node voltages have been measured with respect to the negative pole of the converter. A PC-based user interface (Fig. 13) allows to select a unipolar or bipolar output, to modify duty cycle, switching frequency,  $dV/dt$ , etc. A picture of the most relevant parts of the described setup is reported in Fig. 14, showing the system including the SiC-based converter, the connecting cable and the electrical machine. Since preliminary investigations have shown that duty cycle and switching frequency do not impact the phenomena under investigation, a bipolar supply at 30kHz and 50% duty cycle is used for the whole test campaign. On the other hand,  $dV/dt$  and voltage levels affect both overshoot and voltage distribution, so the validation exercise will focus on such aspects.

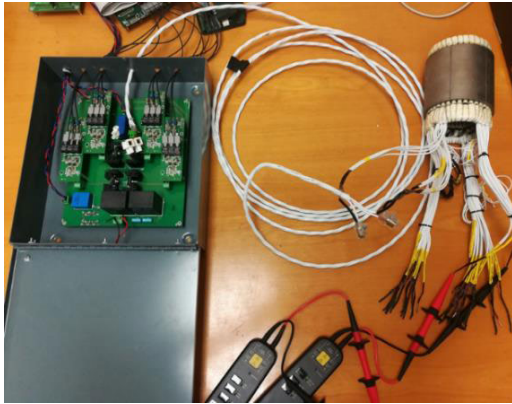


FIGURE 14. SiC-based converter, connecting cable and electrical motor with accessible interturn terminals.

**B. MODEL VALIDATION**

The experimental measurements for model validation have been carried out at reduced DC link voltage values, in order to keep the current below the limit of the SiC MOSFETs. In particular, tests up to 150 V were possible without overcoming the 11 A rating of the WBG devices. In this paper, the results at 100 V and 150 V with bipolar supply are considered. Although the tests are performed at reduced voltage, the rise times of the converter output voltage is only 33 ns at 100 V and 29 ns at 150 V. Under these operating conditions, the overvoltage and the uneven voltage distribution are rather quantifiable, with the resulting waveforms being still quite steep. Figures 15 and 16 show the line to line voltages at 100 V and 150 V, respectively. An excellent match can be observed, especially considering the peak voltage which is the main quantity for designing an insulation system and for estimating PDIVs (see Part II).

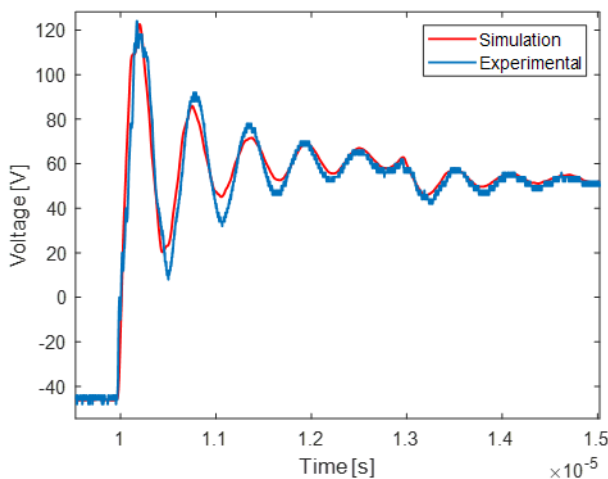


FIGURE 15. Line to line DM voltage at motor terminals at 100 V.

The corresponding node voltages are shown in Figures 17-20. In particular, Fig. 17 and Fig. 18 report the comparison between simulation and experimental node voltages for the 2<sup>nd</sup> and 6<sup>th</sup> turns, respectively, when the DC

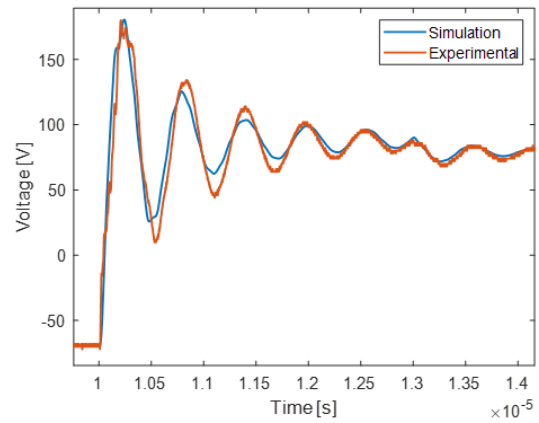


FIGURE 16. Line to line DM voltage at motor terminals at 150 V.

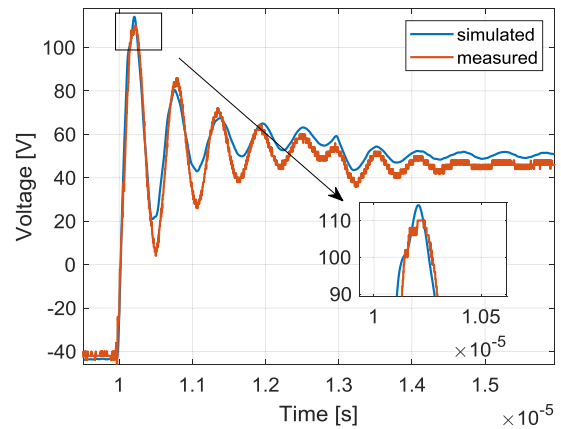


FIGURE 17. 2<sup>nd</sup> turn voltages with 100 V supply

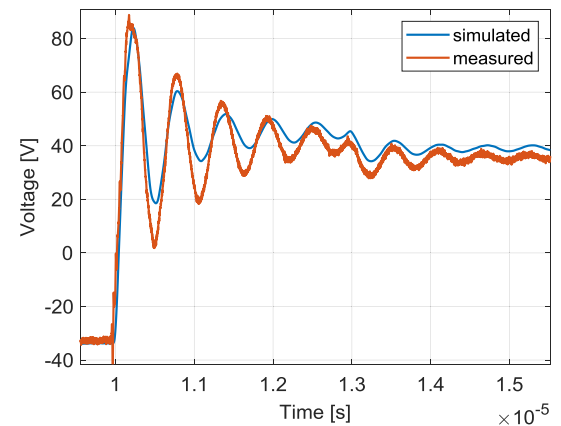


FIGURE 18. 6<sup>th</sup> turn voltages with 100 V supply.

link voltage is set at 100 V. Figures 19 and 20 show the same comparison at 150 V. Also in this case the match is very good, with a negligible error on the 2<sup>nd</sup> turn (<2%) and a maximum error of ≈5% on the 6<sup>th</sup> turn recorded at 150 V.

On the other hand, a small discrepancy can be noticed after the first instants of the pulse on both the line-to-line voltage at the machine terminals and the node voltages. This is due

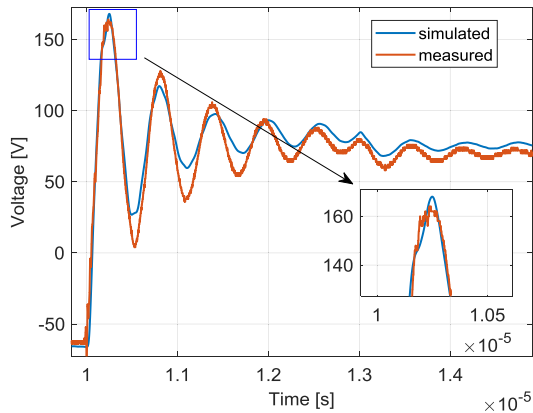


FIGURE 19. 2<sup>nd</sup> turn voltages with 150 V supply.

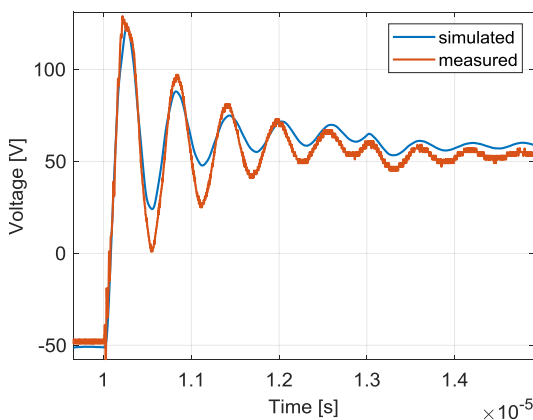


FIGURE 20. 6<sup>th</sup> turn voltages with 150 V supply.

to having adopted an approach which neglects the variation of the equivalent parameters with the frequency during the transient. For the same reason there is a little overestimation of the steady-state values due to a slight overestimation of the lumped parameters modelling the last turns. However, the most significant quantities for the studies carried out in the companion papers (part II and part III) are just the peak voltages at the machine terminals and at its first coil turns, whose values are accurately predicted by the developed comprehensive model. It can also be noticed the similarity between the different waveforms of Figures 15-20: although the cable is quite short, the short rise times provide a notable overshoot and voltage oscillations which can be observed both at machine terminals and within turns.

## VI. CONCLUSION

This paper proposed a modelling approach for the comprehensive analysis of high-frequency challenges in electrical drives designed for aerospace applications, in particular the overvoltage at the machine terminals and the voltage distribution within windings. After a separate description of the models for the estimation of these insulation stress sources, the combined model was detailed. The main benefit of developing a combined, flexible and comprehensive tool

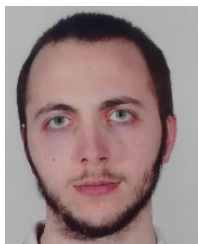
is that both overvoltage at machine terminals and uneven voltage distribution can be calculated simultaneously, without neglecting the voltage overshoot when estimating the voltage distribution (and vice versa). In fact, an accurate calculation of the terminal overvoltage is necessary to provide a good estimation of the voltage within winding turns since its waveform shape can be quite different with respect to the converter output, even with cables of a few meters.

A case study based on a real aerospace application was considered to investigate the model validity and accuracy. Experimental results were performed on a complete system comprising a SiC-based converter, a connecting cable and a machine stator, proving the simulation model accuracy in terms of peak voltages of both the line-to-line terminal voltage and the turn voltage distribution across the first turns, which are the most relevant quantities for the sake of this study as well as for the investigations of the subsequent companion papers. In the forthcoming papers, the effects of different rise times and cable lengths on the inception of partial discharges will be investigated through fast parametric simulation carried out using the proposed combined model. The feasibility of using conventional insulation systems for aircraft applications using SiC drives fed by a  $\pm 270$  V DC bus voltage will be discussed, with the aim of signaling and finding solutions to improve the overall reliability.

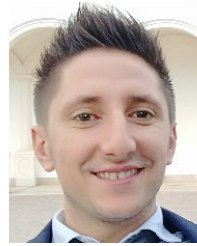
## REFERENCES

- [1] N. K. Bajjuri and A. K. Jain, "Equivalent 3-level PWM: An improved technique to reduce torque ripple in DI-WRIM analyzed as DI-OWIM," *IEEE Trans. Ind. Electron.*, vol. 68, no. 3, pp. 2108–2119, Mar. 2021, doi: 10.1109/TIE.2020.2972440.
- [2] *Insulation Co-Ordination, Part 2: Application Guide*, document IEC 60071-2, 1996.
- [3] A. Greenwood, *Electrical Transients in Power Systems*. New York, NY, USA: Wiley, 1991.
- [4] P. Chowdhuri, *Electromagnetic Transients in Power Systems*, 2nd ed. New York, NY, USA: Research Studies Press, 2004.
- [5] M. J. Melfi, "Low-voltage PWM inverter-fed motor insulation issues," *IEEE Trans. Ind. Appl.*, vol. 42, no. 1, pp. 128–133, Jan. 2006.
- [6] J. L. Guardado and K. J. Cornick, "The effect of coil parameters on the distribution of steep-fronted surges in machine windings," *IEEE Trans. Energy Convers.*, vol. 7, no. 3, pp. 552–559, Sep. 1992.
- [7] S. R. Chalise, S. Grzybowski, and C. D. Taylor, "Accelerated electrical degradation of machine winding insulation," in *Proc. 41st North American Power Symp.*, 2009, pp. 1–6.
- [8] I. Tilea and C. Munteanu, "Motor cable electric parameter effects on the overvoltage phenomenon in inverter driven motors," in *Proc. 8TH Int. Symp. Adv. Topics Electr. Eng. (ATEE)*, Bucharest, Romania, May 2013, pp. 1–6.
- [9] A. F. Moreira, T. A. Lipo, G. Venkataramanan, and S. Bernet, "High-frequency modeling for cable and induction motor overvoltage studies in long cable drives," *IEEE Trans. Ind. Appl.*, vol. 38, no. 5, pp. 1297–1306, Sep. 2002.
- [10] L. Wang, C. N.-M. Ho, F. Canales, and J. Jatskevich, "High-frequency modeling of the long-cable-fed induction motor drive system using TLM approach for predicting overvoltage transients," *IEEE Trans. Power Electron.*, vol. 25, no. 10, pp. 2653–2664, Oct. 2010.
- [11] L. Arnedo and K. Venkatesan, "Pspice simulation for conducted EMI and overvoltage investigations in a PWM induction motor drive system," in *Proc. IEEE Workshop Comput. Power Electron.*, Mayaguez, Puerto Rico, Jun. 2002, pp. 132–137.
- [12] S. De Caro, S. Foti, T. Scimone, A. Testa, G. Scelba, M. Pulvirenti, and S. Russo, "Motor overvoltage mitigation on SiC MOSFET drives exploiting an open-end winding configuration," *IEEE Trans. Power Electron.*, vol. 34, no. 11, pp. 11128–11138, Nov. 2019.

- [13] C. Petrarca, A. Maffucci, V. Tucci, and M. Vitelli, "Analysis of the voltage distribution in a motor stator winding subjected to steep-fronted surge voltages by means of a multiconductor lossy transmission line model," *IEEE Trans. Energy Convers.*, vol. 19, no. 1, pp. 7–17, Mar. 2004.
- [14] A. Krings, G. Paulsson, F. Sahlen, and B. Holmgren, "Experimental investigation of the voltage distribution in form wound windings of large AC machines due to fast transients," in *Proc. 22nd Int. Conf. Electr. Mach. (ICEM)*, Lausanne, Switzerland, Sep. 2016, pp. 1700–1706.
- [15] Y. Xie, J. Zhang, F. Leonardi, A. R. Munoz, M. W. Degner, and F. Liang, "Voltage stress modeling and measurement for random-wound windings driven by inverters," in *Proc. IEEE Int. Electric Mach. Drives Conf. (IEMDC)*, San Diego, CA, USA, May 2019, pp. 1917–1924.
- [16] H. A. Toliyat, G. Suresh, and A. Abur, "Estimation of voltage distribution on the inverter fed random wound induction motor windings supplied through feeder cable," *IEEE Trans. Energy Convers.*, vol. 14, no. 4, pp. 976–981, Dec. 1999.
- [17] M. T. Wright, S. J. Yang, and K. McLeay, "General theory of fast-fronted interturn voltage distribution in electrical machine windings," in *Proc. Inst. Electr. Eng.*, 1983, pp. 257–264.
- [18] Y. Xie, J. Zhang, F. Leonardi, A. R. Munoz, F. Liang, and M. W. Degner, "Modeling and verification of electrical stress in inverter-driven electric machine windings," in *Proc. IEEE Energy Convers. Congr. Exposit. (ECCE)*, Portland, OR, USA, Sep. 2018, pp. 5742–5749.
- [19] G. Suresh, H. A. Toliyat, D. A. Rendusara, and P. N. Enjeti, "Predicting the transient effects of PWM voltage waveform on the stator windings of random wound induction motors," *IEEE Trans. Power Electron.*, vol. 14, no. 1, pp. 23–30, Jan. 1999.
- [20] V. Mihaila, S. Duchesne, and D. Roger, "A simulation method to predict the turn-to-turn voltage spikes in a PWM fed motor winding," *IEEE Trans. Dielectr. Electr. Insul.*, vol. 18, no. 5, pp. 1609–1615, Oct. 2011.
- [21] P. Bidan, T. Lebey, G. Montseny, and J. Saint-Michel, "Transient voltage distribution in inverter fed motor windings: Experimental study and modeling," *IEEE Trans. Power Electron.*, vol. 16, no. 1, pp. 92–100, Jan. 2001.
- [22] J. M. Martinez-Tarifa, H. Amaras-Duarte, and J. Sanz-Feito, "Frequency-domain model for calculation of voltage distribution through random wound coils and its interaction with stray capacitances," *IEEE Trans. Energy Convers.*, vol. 23, no. 3, pp. 742–751, Sep. 2008.
- [23] M. Lukic, P. Giangrande, A. Hebala, S. Nuzzo, and M. Galea, "Review, challenges, and future developments of electric taxiing systems," *IEEE Trans. Transport. Electrific.*, vol. 5, no. 4, pp. 1441–1457, Dec. 2019.
- [24] P. Giangrande, V. Madonna, S. Nuzzo, and M. Galea, "Moving toward a reliability-oriented design approach of low-voltage electrical machines by including insulation thermal aging considerations," *IEEE Trans. Transport. Electrific.*, vol. 6, no. 1, pp. 16–27, Mar. 2020, doi: 10.1109/TTE.2020.2971191.
- [25] G. Skibinski, D. Leggate, and R. Kerkman, "Cable characteristics and their influence on motor over-voltages," in *Proc. Appl. Power Electron. Conf. (APEC)*, Atlanta, GA, USA, 1997, pp. 114–121.
- [26] M. Pastura, S. Nuzzo, M. Kohler, and D. Barater, "Dv/Dt filtering techniques for electric drives: Review and challenges," in *Proc. 45th Annu. Conf. IEEE Ind. Electron. Soc. (IECON)*, Lisbon, Portugal, Oct. 2019, pp. 7088–7093.
- [27] M. Pastura, S. Nuzzo, G. Franceschini, G. Sala, and D. Barater, "Sensitivity analysis on the voltage distribution within windings of electrical machines fed by wide band gap converters," in *Proc. Int. Conf. Electr. Mach. (ICEM)*, Gothenburg, Sweden, Aug. 2020, pp. 1594–1600, doi: 10.1109/ICEM49940.2020.9270958.



**MARCO PASTURA** received the M.Sc. degree in electrical engineering from the University of Pavia, Pavia, Italy, in 2018. He is currently pursuing the Ph.D. degree in "automotive engineering for intelligent mobility" with the Department of Engineering "Enzo Ferrari," University of Modena and Reggio Emilia, Modena, Italy. His research interests are the electrical drives for automotive and aerospace applications with focus on high reliability electrical machines.



**STEFANO NUZZO** (Member, IEEE) received the B.Sc. and M.Sc. degrees in electrical engineering from the University of Pisa, Pisa, Italy, in 2011 and 2014, respectively, and the Ph.D. degree in electrical engineering from the University of Nottingham, Nottingham, U.K., in 2018, where he worked also as a Research Fellow with the Power Electronics, Machines and Control (PEMC) Group. Since January 2019, he has been a Research Fellow with the Department of Engineering "Enzo Ferrari," University of Modena and Reggio, Modena, Italy. His research interests are the analysis, modeling and optimizations of electrical machines, with focus on salient-pole synchronous generators and brushless excitation systems for industrial power generation applications. He is also involved in a number of projects related to the more electric aircraft initiative and associated fields.

Dr. Nuzzo is a Member of the IEEE Industrial Electronics Society (IES) and the IEEE Industry Applications Society (IAS). He constantly serves the scientific community as a reviewer for several journals and conferences.



**FABIO IMMOVILLI** (Senior Member, IEEE) received the M.S. degree and the Ph.D. degree in mechatronic engineering from the University of Modena and Reggio Emilia, Italy, in 2006 and 2011, respectively. Since November 2019, he has been an Associate Professor of electric converters, machines and drives with the Department of Sciences and Methods for Engineering, University of Modena and Reggio Emilia, Italy. He is the author or coauthor of more than 40 technical papers. His research interests include electric machine condition monitoring, electric power converters, machines for energy conversion from renewable energy sources and thermoacoustics.



**ANDREA TOSCANI** received the M.S. degree (*cum laude*) in electronic engineering and the Ph.D. degree in information technology from the University of Parma, Italy, in 2004 and 2008, respectively. Since 2004, he has been with the Department of Information Engineering (now Dept. of Engineering and Architecture), University of Parma. He is currently a Research Fellow. His research activity is mainly focused on power electronics, high-performance electric drives and diagnostic techniques for industrial electric systems. He is the author of two patents.



**ALBERTO RUMI** (Student Member, IEEE) was born in Lugo (RA), Italy, in April 1994. He received the B.Sc. and M.S. degrees in electrical engineering from the University of Bologna, Italy, in 2016 and 2019, respectively, where he is currently pursuing the Ph.D. degree in biomedical, electrical and systems engineering. His research interests include diagnosis of insulation systems by partial discharge analysis, the study of the ageing mechanisms of rotating electrical machines and reliability of inverter-fed low voltage motors, especially in the aeronautical and automotive fields.



**ANDREA CAVALLINI** (Senior Member, IEEE) was born in December 1963. He received the master's degree in electrical engineering and the Ph.D. degree in electrical engineering from the University of Bologna, in 1990 and 1995, respectively. He was a Researcher with Ferrara University, from 1995 to 1998. Since 1998, he has been an Associate Professor with Bologna University. He was cofounder of spinoff company Techimp HQ Spa. His research interests are diagnosis of insulation systems by partial discharge analysis, reliability of electrical systems and artificial intelligence. He is the author or coauthor of more than 250 international papers and holds 16 international patents. He is a member of IEC TC 2/MT 10 and project leader of IEC 60034-18-41 Ed. 2.



**GIOVANNI FRANCESCHINI** received the master's degree in electronic engineering from the University of Bologna, Bologna, Italy. From 1990 to 2018, he was with the Department of Information Engineering, University of Parma, Parma, Italy, where he was a Full Professor of electric machines and drives, also holding the position of Vice Rector of the University of Parma, and before the Head of the Department of Information Engineering. In 2018, he joined the Department of Engineering Enzo Ferrari at the University of Modena and Reggio, Italy, where he is currently a Full Professor of electric machines and drives. His research interests include high-performance electric drives and diagnostic techniques for industrial electric system. He was the Coordinator of the European Project ALEA, to achieve complete and accurate lifetime models for electrical drives in aerospace applications. He is the author of more than 150 technical papers.



**DAVIDE BARATER** (Member, IEEE) received the master's degree in electronic engineering and the Ph.D. degree in information technology from the University of Parma, Italy, in 2009 and 2014, respectively.

He was an Honorary Scholar at the University of Nottingham, U.K., in 2012, and a Visiting Researcher at the University of Kiel, DE, in 2015. He is currently an Assistant Professor with the Department of Engineering "Enzo Ferrari", University of Modena and Reggio Emilia, Italy. His research area is focused on power electronics for e-mobility and motor drives. He is the Coordinator of two European Project: RAISE, that evaluates the impact of the high voltage gradients, introduced by the fast commutations of new wide bandgap power devices (SiC, GaN), on the life time of electrical motor insulation systems; AUTO-MEA, that aims to develop electrical motors and drives for next generation of electrical mobility. In particular, novel solutions for windings structures and cooling systems for improved power density, efficiency and increased frequency operation.

Dr. Barater is an Associate Editor of the IEEE TRANSACTIONS ON INDUSTRY APPLICATIONS and author or coauthor of more than 60 international papers.

...